Journal of Inorganic Biochemistry 277 (2026) 113230

Contents lists available at ScienceDirect

Journal of Inorganic Biochemistry

journal homepage: www.elsevier.com/locate/jinorgbio

Lewis acid-promoted self-sensitized photocatalytic CO_2 reduction by a bimetallic Fe complex☆

Matthias Huber, Corinna R. Hess *

Faculty of Chemistry and Pharmacy, University of Regensburg, 93053 Regensburg, Germany

ARTICLE INFO

Keywords:
Bimetallic complex
Redox properties
self-sensitized photocatalysis
CO_2 reduction

ABSTRACT

The modified macrocyclic Mabiq ligand, ^{MeO}**Mbq**, contains two methoxy groups at the outer biquinazoline unit that allow for coordination of a second metal ion in the absence of auxiliary ligands. A series of bimetallic **MFe^{MeO}Mbq** complexes was synthesized, containing Na, Mg, Fe or Zn adjacent to a centrally bound ferrous ion. The redox properties correlate with the Lewis acidity of the supporting metal. Both Fe and Zn in the outer site boost the photocatalytic CO_2 reduction activity of the central ferrous site. The bimetallic **ZnFe^{MeO}Mbq** achieves up to 140 TONs (1 h) for selective CO_2 to CO conversion in a self-sensitized process.

1. Introduction

Multimetallic motifs are commonly found in the active sites of metalloenzymes; synergistic interactions between the metal centers are key to efficient catalysis[1–4]. In several cases, reactivity is achieved using a redox active transition metal as the catalytic center, in combination with a redox-inert, Lewis acidic metal ion in a supporting role. Such motifs are found in the active sites of e.g., Photosystem II[5], CuZn superoxide dismutase[6,7], and Ni,Fe-Carbon Monoxide Dehydrogenases (CODHs)[8]. The supporting metals in these enzymes — Ca, Zn and Fe respectively in the aforementioned examples — often assume multiple functions whereby they act as structural partners, modulate the redox potential of the catalytic metal center, alter the pK_a of intermediates, and/or stabilize coordinated small molecules. Our interest lies in the development of CO_2 reduction catalysts, and in that regard, the Ni,Fe-CODH active site (Scheme 1) exemplifies the various ways in which a Lewis acidic metal site can aid catalysis[4,8–10]. The redox active Ni ion in the active site C-cluster coordinates the C-atom of CO_2 and transfers electrons to the substrate. The neighboring Lewis acidic Fe ion assists CO_2 activation by coordinating its O-atom and pulling electron density away from the molecule. The Fe center additionally regulates the potential of the Ni site.

The varying influences of Lewis acidic metals on reactivity have likewise been demonstrated in synthetic bimetallic motifs for CO_2 reduction[9,11–15]. These systems include complexes in which CO_2 binds to both the catalytic redox active metal ion and the LA (as in CODH), as well as compounds where the supporting metal is further removed from the catalytic metal center and presumed not to interact with the substrate. In the latter case, the supporting metal can still impact catalysis through electrostatic effects.

We recently reported on self-sensitized photocatalytic CO_2 reduction by a bimetallic CuFe-Mabiq complex ([Cu(Xantphos)Fe(Mbq)(OTf)$_2$] (**XCuFeMbq**), Scheme 1; Mabiq = **Mbq** = 2–4:6–8-bis(3,3,4,4-tetramethyldihydropyrrolo)-10–15-(2,2'-biquinazolino)-[15]-1,3,5,8,10,14-hexaene-1,3,7,9,11,14-N$_6$)[16]. The redox inert Cu-Xantphos unit has a marked effect on the redox properties of the Fe center, and consequently, alters the pathway for electrocatalytic CO_2 reduction vs. that of the monometallic **FeMbq**. Moreover, the Cu influences the photochemical behavior of **FeMbq**[17]. The altered photochemistry represents another way in which supporting metals can influence reactivity, and in the case of **XCuFeMbq**, underpins its ability to photocatalyze CO_2 reduction in the absence of an added photosensitizer. We have now synthesized a **Mbq** variant, ^{MeO}**Mbq** (2–4:6–8-bis(3,3,4,4-tetramethyldihydropyrrolo)-10–15-(8,8'-dimethoxy-2,2'-biquinazolino)-[15]-1,3,5,8,10,14-hexaene-1,3,7,9,11,14-N$_6$; Scheme 1), that permits examination of a wider array of metal ion combinations. Here we present a series of **MFe^{MeO}Mbq** complexes (Scheme 1) containing varying Lewis acidic metals (Na, Mg, Fe, Zn) adjacent to a centrally bound ferrous ion. The redox, photochemical, and photocatalytic properties of the **MFe^{MeO}Mbq** complexes demonstrate the ways in which a Lewis acid can support the catalytic center, including in light-driven reactions.

☆ This article is part of a Special issue entitled: 'Harry Gray Special Issue' published in Journal of Inorganic Biochemistry.

* Corresponding author.
E-mail address: corinna.hess@ur.de (C.R. Hess).

https://doi.org/10.1016/j.jinorgbio.2026.113230
Received 16 November 2025; Received in revised form 22 December 2025; Accepted 11 January 2026
Available online 12 January 2026

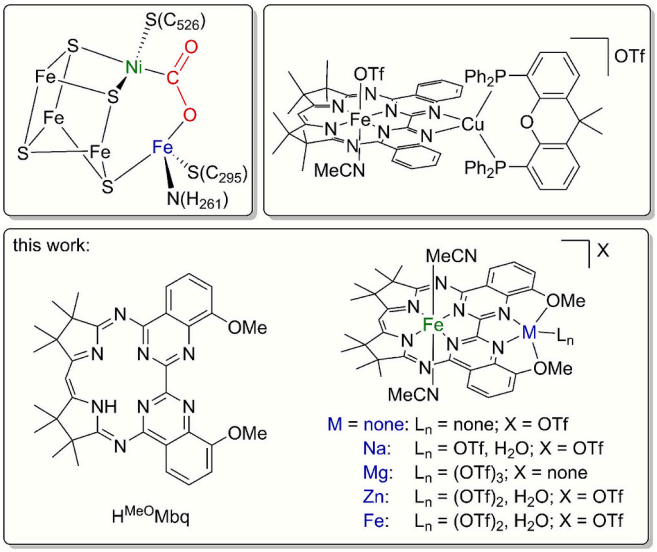

Scheme 1. Top left: Ni,Fe-CODH active site[8]; Top right: **XCuFeMbq** [16]; Bottom: Schematic representation of **H^{MeO}Mbq** (left) and its metal complexes (right).

2. Results and discussion

The ability to coordinate two different metals is a distinctive feature of our original Mbq ligand. However, since the biquinazoline unit provides only two N-donors for the outer metal ion, auxiliary ligands are generally needed to complete the coordination sphere around the second metal. So far, we have primarily examined peripheral motifs using Cu^{I} in combination with phosphines[16,18]; several other metal/ligand combinations proved to be coordinatively unstable. To enhance the affinity of the outer biquinazoline unit for diverse metal ions, and potentially eliminate the need for auxiliary ligands, we generated the new ligand variant, **H^{MeO}Mbq**. **H^{MeO}Mbq** contains two methoxy groups at the 8,8' positions of the biquinazoline moiety (Scheme 1) as additional donor groups. The synthesis of the modified ligand follows the same procedure as for **HMbq**,[19] but using 2-amino-3-methoxybenzamide instead of 2-aminobenzamide as the starting material (Scheme S1).

The solid-state structure and solution state properties of the iron-containing complex, [Fe(^{MeO}Mbq)(MeCN)$_2$]OTf (**Fe^{MeO}Mbq**; Fig. S1-S5) are virtually identical to that of our previously reported **FeMbq** ([Fe(Mbq)(MeCN)$_2$]OTf)[16]. The electron donating methoxy groups lead to an upfield shift of all ^{1}H NMR signals, with the strongest influence on the resonances of the biquinazoline moiety (Fig. S3). The absorption spectrum of **Fe^{MeO}Mbq** features the same bands as that of **FeMbq**, with only slightly altered λ_{max} and intensities (Fig. 1 and Fig. S4).

We subsequently examined the coordination of NaOTf and Mg(OTf)$_2$ to **Fe^{MeO}Mbq** in the absence of auxiliary ligands. With NaOTf, one equivalent of the triflate salt was sufficient to generate the bimetallic **NaFe^{MeO}Mbq**, as indicated by NMR spectroscopy (Fig. S6). However, 5 equiv of Mg(OTf)$_2$ are required to fully convert the monometallic complex to the binuclear **MgFe^{MeO}Mbq** (Fig. S7-S8) in solution. Nonetheless, recrystallization of the crude product yielded a mixture of mono- and bimetallic complexes together with uncoordinated Mg(OTf)$_2$. We therefore could not cleanly isolate **MgFe^{MeO}Mbq** in the solid form. The bimetallic complex was thus subsequently generated in situ upon addition of 5 equiv of Mg(OTf)$_2$ to **Fe^{MeO}Mbq**.

A library of bimetallic complexes (**NaFe^{MeO}Mbq**, **MgFe^{MeO}Mbq**, **Fe$_2^{MeO}$Mbq**, **ZnFe^{MeO}Mbq**) was generated using the above-described approach, mixing **Fe^{MeO}Mbq** with metal triflates (NaOTf, Mg(OTf)$_2$, Zn(OTf)$_2$, and Fe(MeCN)$_2$(OTf)$_2$). Solutions of the complexes generated in this manner were used for analytical and reactivity studies. The bimetallic complexes containing the closed shell metals (Na, Mg, Zn) in the outer site were generated using a 1:5 ratio of **Fe^{MeO}Mbq**:triflate salts. The coordination of the neighboring metal results in noticeable NMR spectral changes compared to that of **Fe^{MeO}Mbq** (Fig. S8-S11), particularly for the resonances assigned to the biquinazoline and diketiminate moiety and the methoxy groups (Fig. S11). The absence of signals associated with the monometallic complex evidences the quantitative formation of the bimetallic complexes in solution. The absorption spectra (MeCN) of the complexes containing Na and Mg in the outer position closely resemble that of **Fe^{MeO}Mbq**, with a distinctive set of bands in the visible region at λ_{max} = 620 – 660 nm (Fig. 1). These transitions are significantly red-shifted in the spectrum of **ZnFe^{MeO}Mbq** (λ_{max} = 709 nm, Fig. 1). Addition of Fe(MeCN)$_2$(OTf)$_2$ yields the paramagnetic **Fe$_2^{MeO}$Mbq**, and formation of the bimetallic complex was therefore examined by absorption spectroscopy. Spectral changes upon titration of a solution of **Fe^{MeO}Mbq** with varying amounts of Fe-triflate suggest that a larger excess of the latter is required to saturate the peripheral binding site (Fig. S12). The spectrum of **Fe$_2^{MeO}$Mbq** generated upon addition of 20 equiv Fe(MeCN)$_2$(OTf)$_2$ features a set of transitions with λ_{max} = 700 nm (Fig. 1).

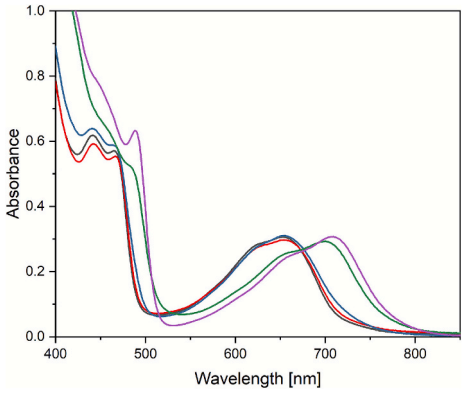

Fig. 1. UV/Vis spectra (50 μM) of **Fe^{MeO}Mbq** (black), **NaFe^{MeO}Mbq** (red), **MgFe^{MeO}Mbq** (blue), **Fe$_2^{MeO}$Mbq** (green), and **ZnFe^{MeO}Mbq** (purple) in MeCN. 5 equiv (**NaFe^{MeO}Mbq**, **MgFe^{MeO}Mbq**, **ZnFe^{MeO}Mbq**) or 20 equiv (**Fe$_2^{MeO}$Mbq**) of the metal-triflate were used to generate the complexes.

Solid-state structures of all complexes also were obtained (structure of MgFe complex shown in Fig. 2; for the other structures, see Fig. S5, S13-S16). The coordination environment around the centrally-bound Fe-center is analogous to the monometallic **Fe^{MeO}Mbq**, i.e., the Fe is ligated by four equatorial ^{MeO}**Mbq** N-donors and two axial MeCN ligands. The peripheral metal is coordinated either by two (Na) or three (Mg, Zn, Fe) additional ligands, either OTf or H_2O (the latter stemming from residual water in the solvent, MeCN). The M-O^{OTf} and M-O^{H2O} bond lengths range from 1.97 to 2.31 Å (Table S5), while the M-O^{MeO} distances are significantly longer (2.60-2.78 Å). The methoxy groups bend slightly towards the outer metal ion, evidencing an interaction despite the long M-O^{MeO} distances. The limited flexibility and the long distance between the two methoxy groups surely impair the affinity of the ligand towards a second metal, which may explain the poor stability of **MgFe^{MeO}Mbq** with respect to recrystallization.

The redox potentials of the **MFe^{MeO}Mbq** series are strongly dependent on the nature of the outer metal ion. The CV of the monometallic **Fe^{MeO}Mbq** is nearly identical to that of **FeMbq**; the electron-donating methoxy groups lead to minimal shifts of the redox potentials, ~20 mV more negative compared to those of **FeMbq** (Fig. 3). The CVs of the bimetallic complexes likewise exhibit one metal-centered oxidative couple, and two reductive couples that are likely ligand-centered (Fig. 3, Fig. S17-S18). A third reductive event could be observed in the CVs of **Fe^{MeO}Mbq**, **NaFe^{MeO}Mbq** and **MgFe^{MeO}Mbq**, which is irreversible for the latter. However, in the case of **ZnFe^{MeO}Mbq** and **Fe$_2^{MeO}$Mbq**, metallic deposits formed on the electrode surface upon scanning beyond the second reduction, stemming from the excess Zn- or Fe-triflates in

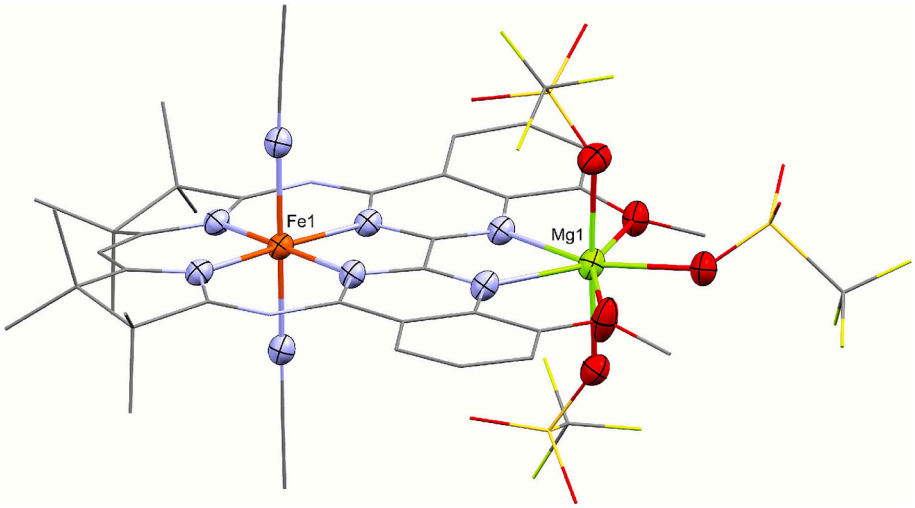

Fig. 2. Molecular structure of **MgFe^{MeO}Mbq**. Ellipsoids are shown at 50% probability level and hydrogen atoms as well as disorder of one methoxy group are omitted for clarity.

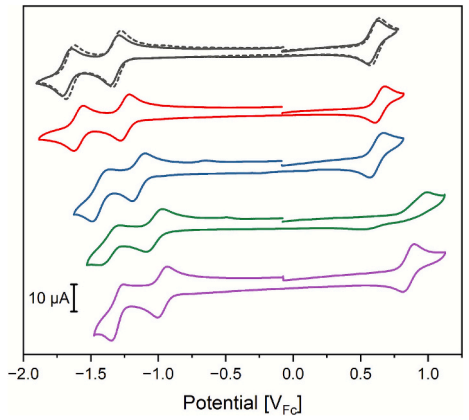

Fig. 3. CVs of a 0.5 mM solution of **FeMbq** (black, dashed), **Fe^{MeO}Mbq** (black, solid), **NaFe^{MeO}Mbq** (red), **MgFe^{MeO}Mbq** (blue), **Fe$_2^{MeO}$Mbq** (green), and **ZnFe^{MeO}Mbq** (purple) in MeCN (0.1 M [(*n*-Bu)$_4$N]PF$_6$). 5 equiv (**NaFe^{MeO}Mbq**, **MgFe^{MeO}Mbq**, **ZnFe^{MeO}Mbq**) or 20 equiv (**Fe$_2^{MeO}$Mbq**) of the metal-triflate were used to generate the complexes.

solution.

The second metal in the **MFe^{MeO}Mbq** series leads to an anodic shift in the redox potentials that increase in the order $Na^+ < Mg^{2+} < Fe^{2+} < Zn^{2+}$ and thereby correlate with the Lewis acid strength of the outer metal (Table 1). Despite small differences in Lewis acidity (Mg^{2+}: 0.337, Fe^{2+}: 0.352, Zn^{2+}: 0.405)[20], the redox potentials of **MgFe^{MeO}Mbq** and **ZnFe^{MeO}Mbq** differ by up to 220 mV. The proximity of the metal cation to the biquinazoline moiety may play an amplifying role: the solid-state structures of the bimetallic complexes show decreasing M-N bond lengths from Mg to Fe to Zn. Therefore, the Zn ion pulls more electron density from the ^{MeO}**Mbq** ligand and leads to a larger anodic shift of the redox potentials. Overall, the **Fe^{MeO}Mbq** potentials can be tuned over a wide range of up to 380 mV through the addition of metal triflates at the neighboring coordination site. Such large effects on redox potentials also have been observed upon coordination of cations in other metal complexes, as a result of changes in the local electric fields[21].

Table 1
Comparison of redox potentials of the complexes in MeCN.

Complex	[Fe(Mbq)]$^{-/2-}$	Mbq$^{\bullet-}$/Mbq^{2-}	Mbq/Mbq$^{\bullet-}$	Fe$^{III/II}$
FeMbq	−2.39 V_{Fc}	−1.67 V_{Fc}	−1.31 V_{Fc}	0.60 V_{Fc}
Fe^{MeO}Mbq	−2.41 V_{Fc}	−1.68 V_{Fc}	−1.33 V_{Fc}	0.59 V_{Fc}
NaFe^{MeO}Mbq	−2.21 V_{Fc}	−1.59 V_{Fc}	−1.26 V_{Fc}	0.63 V_{Fc}
MgFe^{MeO}Mbq	−1.87 V_{Fc}[a]	−1.42 V_{Fc}	−1.13 V_{Fc}	0.64 V_{Fc}
Fe$_2^{MeO}$Mbq		−1.36 V_{Fc}	−1.03 V_{Fc}	0.75 V_{Fc}
ZnFe^{MeO}Mbq		−1.31 V_{Fc}	−0.97 V_{Fc}	0.85 V_{Fc}

Potentials are based on CVs run in duplicate with values ± 0 – 31 mV.
[a] Peak potential is reported due to irreversibility

The photocatalytic activity of the series of iron containing ^{MeO}**Mbq** complexes for the CO_2 reduction reaction (CO_2RR) also is dependent on the nature of the outer metal ion. All compounds selectively yield CO as a product upon irradiation (λ_{irr} = 455 nm) of solutions containing the metal-^{MeO}**Mbq** complexes, CO_2, PhOH as the proton source and BIH as a sacrificial donor ([complex] = 2 μM, [PhOH] = 170 μM, [BIH] = 100 mM; see Table S6-S7 for full set of data from all experiments, including control experiments). Photocatalysis experiments were carried out in either pure MeCN or a 1:1 THF/MeCN mixture, in consideration of the stability of the complexes or the reduced forms in these solvents. H_2 was not generated in appreciable amounts in any of the catalytic experiments (Table S6).

The monometallic **Fe^{MeO}Mbq** generated 81 nM CO after 1 h reaction time in the THF/MeCN mixture, corresponding to 20 TONs, and slightly higher amounts (244 nM CO) in pure MeCN (Fig. 4A). As previously observed for **FeMbq**, the CO_2RR activity of the monometallic compound is fairly low in the absence of an added photosensitizer[16]. Na has no effect on the photocatalytic activity (19 TONs, Fig. 4A), whereas **MgFe^{MeO}Mbq** produces slightly more CO (38 TONs, Fig. 4A) under analogous reaction conditions. However, the yields of CO produced by both **Fe$_2^{MeO}$Mbq** and **ZnFe^{MeO}Mbq** were significantly higher. After 1 h reaction time, the diiron complex — generated using 20 equiv of added $Fe(MeCN)_2(OTf)_2$ — achieved 146 TONs in MeCN, and the ZnFe complex achieved 97 or 144 TONs (Fig. 4A) depending on the solvent. For **ZnFe^{MeO}Mbq**, we also examined the photocatalytic activity over a longer period (5 h, Figure S20 and Table S8). The catalyst remained active during this time period, with 2.5-fold more CO produced. Control experiments with added Hg (Table S8) confirm that the activity is not due to nanoparticles or metallic deposits, and no activity is observed using $Zn(OTf)_2$ with $[Ru(bpy)_3]^{2+}$ as a photosensitizer (Table S6). Overall, our results show that the activity of the bimetallic complexes tracks reasonably well with the redox effects of the outer metal ion and establish the **Fe$_2$- and ZnFe^{MeO}Mbq** complexes as self-sensitized CO_2 reduction catalysts.

Interestingly, there is no correlative effect of the outer metal on the photochemical properties of the metal-^{MeO}**Mbq** compounds. The one-electron photoreduction of the various complexes (except for the

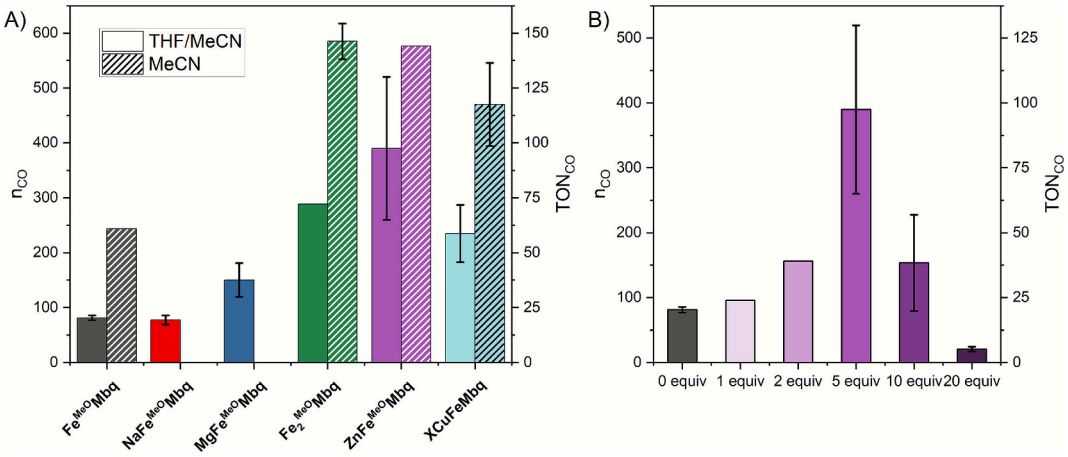

Fig. 4. A) Amount of CO produced in photocatalytic studies with **Fe^{MeO}Mbq** (black), **$NaFe^{MeO}$Mbq** (red), **$MgFe^{MeO}$Mbq** (blue), **Fe_2^{MeO}Mbq** (green), **$ZnFe^{MeO}$Mbq** (purple), and **XCuFeMbq** (cyan). Bimetallic compounds were generated using a 1:5 **Fe^{MeO}Mbq**:metal triflate ratio except for **Fe_2^{MeO}Mbq** which was generated using a 1:20 ratio. Standard conditions: 2 μM catalyst, 170 μM PhOH, 100 mM BIH, solution purged with CO_2 for 2 min. B) TONs for CO produced by solutions of **Fe^{MeO}Mbq** with varying equiv of added $Zn(OTf)_2$ (in 1:1 THF:MeCN).

diiron compound, vide infra) was examined using Et_3N as a sacrificial donor, with irradiation at 455 nm. The spectra of the initial photoreduction product generated in all cases resemble, but are not identical to, that of the formal Fe^{I}-Mbq, and the photoconversions proceed cleanly as indicated by clear isosbestic points (Fig. 5 and Fig. S21-S24). For **Fe^{MeO}Mbq**, **$NaFe^{MeO}$Mbq** and **$ZnFe^{MeO}$Mbq** the quantum yields associated with the initial photoreduction process vary minimally, with values in the range of 5.5 to 11.4×10^{-5} (Table S9). Only the photoconversion of **$MgFe^{MeO}$Mbq** proceeds discernably slower (1.8×10^{-5}; Table S9). Therefore, despite the high CO_2RR photoactivity of **$ZnFe^{MeO}$Mbq**, the photoreduction does not proceed any faster than for **Fe^{MeO}Mbq**, nor are any different photoreduction products observed.

The absorption spectrum of the **Fe_2^{MeO}Mbq** complex is already altered by the presence of Et_3N. Thus, the photoreduction was examined in MeCN using BIH as a sacrificial donor (Fig. S23), wherein clean conversion of the initial Fe_2^{II} form is likewise observed. The spectrum of the initial photoreduction product also resembles that of Fe^{I}-Mbq, and the timescale for formation of the reduced form is comparable to what was observed for **FeMbq** under identical conditions[17].

Overall, the photoreduction quantum yields for the bimetallic compounds do not correlate with their redox potentials. The photochemical behavior of the bimetallic **^{MeO}Mbq** complexes is contrary to what we observed for **XCuFeMbq**[17], where the neighboring Cu center

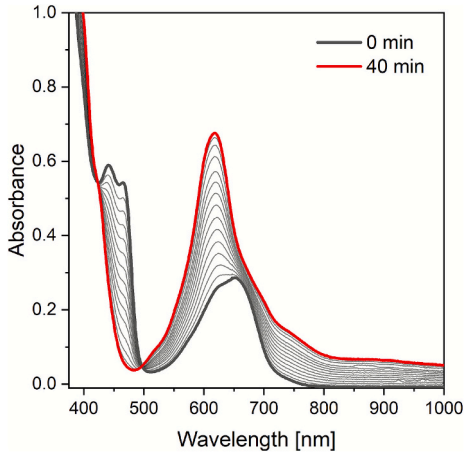

Fig. 5. Representative UV/Vis absorption spectra recorded during the photoreduction of **Fe^{MeO}Mbq** in the presence of 2000 equiv (100 mM) Et_3N as a sacrificial reductant in THF/MeCN.

enhanced the photocatalytic activity and had a significant impact on the photoreduction process. Electrostatic effects of the supporting metals in the **MFe^{MeO}Mbq** are insufficient to alter the excited state properties and quantum yields for the initial photoreduction process. The redox potentials and/or excited state properties of down-stream intermediates of the **Fe_2-** and **$ZnFe^{MeO}$Mbq** may thus account for their increased catalytic activity.

Since **$ZnFe^{MeO}$Mbq** gave the highest photocatalytic CO_2 reduction activity — even in solutions with low amounts of added $Zn(OTf)_2$ compared to the diiron compound — we further examined the influence of added Zn-triflate on the reaction (Fig. 4B). The influence of a supporting metal on CO_2 reduction often can be attributed to the ability of the neighboring LA to coordinate to a CO_2 adduct generated at the catalytic metal (vide supra)[11]. The Zn ion in the outer biquinazoline site of **$ZnFe^{MeO}$Mbq** is too far removed from the **Fe^{MeO}Mbq** to effectively and directly interact with a centrally bound CO_2 molecule (Zn···Fe = 5.43 Å). However, given the amount of $Zn(OTf)_2$ used in all the above-described experiments (5 equiv), we could not exclude the possibility that a zinc ion might associate with an Fe-bound CO_2 species via an external interaction. The photocatalytic CO_2RR activity is indeed dependent on the **Fe^{MeO}Mbq**:$Zn(OTf)_2$ stoichiometry used (Fig. 4B, Table S7), with the maximum activity achieved using a 1:5 ratio of the two metal compounds, respectively. This corresponds to the Zn:Fe ratio required for complete conversion of the monometallic to bimetallic complex in THF/MeCN, as indicated by the spectroscopic data (vide supra and Fig. S25). The TONs are dramatically reduced in the presence of 20 equiv $Zn(OTf)_2$ (5 TONs), implying that any additional interaction of Zn^{2+} with the metal-**^{MeO}Mbq** species is unfavorable. Therefore, the enhanced catalytic activity of **$ZnFe^{MeO}$Mbq** seems to be predominantly due to the neighboring, biquinazoline bound zinc ion.

3. Conclusions

Our findings show that the properties of the central metal-**^{MeO}Mbq** site are influenced by the Lewis acidity of the supporting metals. Fe and Zn have the largest impact on both the redox and photocatalytic properties. The **$ZnFe^{MeO}$Mbq** is better behaved, since the Zn ion has a higher affinity for and stability at the outer metal binding site. The self-sensitized photocatalytic CO_2 reduction activity of the ZnFe complex is comparable to, if not better, than that of the previously reported **XCuFeMbq**.

Many heteroleptic P_2N_2-Cu complexes themselves are photoactive. In our case, the Cu-Xantphos unit of **XCuFeMbq** had no effect on the excited state lifetimes, but we hypothesized that changes to redox

properties or reorganization energies due to the Cu site might be responsible for the altered photoactivity of the bimetallic compound [17]. The combined structural, spectroscopic, redox, and photochemical properties across the series of **MFe^{MeO}Mbq** complexes clearly demonstrate that enhanced photocatalytic activity does not rely on the incorporation of another photoactive metal center; and steric factors do not seem to play a role. Instead, self-sensitized catalysis can already be promoted to an extent via modulation of redox potentials with appropriate Lewis acidic metal ions.

TONs as high as 1000 have recently been reported for self-sensitized CO_2 reduction by molecular dipyrrin-amide-Cu (2 h reaction time; in MeCN/H_2O) and CNC pincer Ni complexes (72 h reaction time; in MeCN), whereby the latter complex generates both formate and CO [22,23]. The maximum TONs achieved by our most active **MFe^{MeO}Mbq** catalysts are lower, but the CO_2RR by our **MFe^{MeO}Mbq** system is highly selective. Reports of selective self-sensitized CO_2 reduction by first-row transition metal complexes remain rare. The TONs reported for the Cu and Ni complexes also were highly dependent on factors such as proton source and solvent — which we have yet to examine; and select ligand modifications resulted in the high self-sensitized activity of the dipyrrin-amide and CNC pincer catalysts. Further modifications to the biquinazoline unit of **^{MeO}Mbq** will be directed at increasing the metal affinity of the outer site and altered photochemical properties. Overall, our findings already demonstrate that the bimetallic Mbq compounds offer highly promising platforms for development of self-sensitized photocatalysts and examination of cooperative effects on photoactivity.

CRediT authorship contribution statement

Matthias Huber: Writing – review & editing, Writing – original draft, Visualization, Validation, Methodology, Investigation, Formal analysis. **Corinna R. Hess:** Writing – review & editing, Writing – original draft, Visualization, Validation, Supervision, Resources, Project administration, Methodology, Funding acquisition, Conceptualization.

Declaration of competing interest

The author declares no competing financial interest.

Acknowledgements

Research reported in this publication was supported by the Deutsche Forschungsgemeinschaft (DFG): 426785626 (CRH and MH), 507868493 (CRH).

Appendix A. Supplementary data

Supplementary data to this article can be found online at https://doi.org/10.1016/j.jinorgbio.2026.113230.

Data availability

Crystallographic data for **Fe^{MeO}Mbq**, **NaFe^{MeO}Mbq**, **MgFe^{MeO}Mbq**, **Fe$_2^{MeO}$Mbq**, and **ZnFe^{MeO}Mbq** has been deposited at the CCDC under 2503016, 2503018, 2503023, 2503025, 2503026. All other data will be made available on request.

References

[1] A.C. Ghosh, C. Duboc, M. Gennari, Synergy between metals for small molecule activation: Enzymes and bio-inspired complexes, Coord. Chem. Rev. 428 (2021) 213606, https://doi.org/10.1016/j.ccr.2020.213606.
[2] N. Sträter, W.N. Lipscomb, T. Klabunde, B. Krebs, Two-metal ion catalysis in enzymatic acyl- and phosphoryl-transfer reactions, Angew. Chem. Int. Ed. Eng. 35 (1996) 2024–2055, https://doi.org/10.1002/anie.199620241.
[3] D.E. Wilcox, Binuclear metallohydrolases, Chem. Rev. 96 (1996) 2435–2458, https://doi.org/10.1021/cr950043b.
[4] H.S. Shafaat, J.Y. Yang, Uniting biological and chemical strategies for selective CO_2 reduction, Nat. Catal. 4 (2021) 928–933, https://doi.org/10.1038/s41929-021-00683-1.
[5] D. Shevela, J.F. Kern, G. Govindjee, J. Messinger, Solar energy conversion by photosystem II: principles and structures, Photosynth. Res. 156 (2023) 279–307, https://doi.org/10.1007/s11120-022-00991-y.
[6] J.A. Tainer, E.D. Getzoff, J.S. Richardson, D.C. Richardson, Structure and mechanism of copper, zinc superoxide dismutase, Nature 306 (1983) 284–287, https://doi.org/10.1038/306284a0.
[7] L.M. Ellerby, D.E. Cabelli, J.A. Graden, J.S. Valentine, Copper−zinc superoxide dismutase: why not pH-dependent? J. Am. Chem. Soc. 118 (1996) 6556–6561, https://doi.org/10.1021/ja953845x.
[8] M. Can, F.A. Armstrong, S.W. Ragsdale, Structure, function, and mechanism of the nickel metalloenzymes, CO dehydrogenase, and acetyl-CoA synthase, Chem. Rev. 114 (2014) 4149–4174, https://doi.org/10.1021/cr400461p.
[9] P. Gotico, Z. Halime, W. Leibl, A. Aukauloo, Bimetallic molecular catalyst design for carbon dioxide reduction, Chempluschem 88 (2023) e202300222, https://doi.org/10.1002/cplu.202300222.
[10] M. Huber, C.R. Hess, Transferring enzyme features to molecular CO_2 reduction catalysts, Curr. Opin. Chem. Biol. 83 (2024) 102540, https://doi.org/10.1016/j.cbpa.2024.102540.
[11] M. Pérez-Jiménez, H. Corona, F. de La Cruz-Martínez, J. Campos, Donor-acceptor activation of carbon dioxide, Chem. Eur. J. 29 (2023) e202301428, https://doi.org/10.1002/chem.202301428.
[12] S. Wolff, V. Pelmenschikov, R. Müller, M. Ertegi, B. Cula, M. Kaupp, C. Limberg, Controlling the activation at Ni^{II}-CO_2^{2-} moieties through lewis acid interactions in the second coordination sphere, Chem. Eur. J. 30 (2024) e202303112, https://doi.org/10.1002/chem.202303112.
[13] S. Wolff, A. Hofmann, K.B. Krause, K. Weisser, B. Cula, T. Lohmiller, C. Herwig, C. Limberg, Mimicking the CO_2-bound state of the [Ni,Fe]-CO dehydrogenase, Angew. Chem. Int. Ed. 64 (2025) e202419675, https://doi.org/10.1002/anie.202419675.
[14] A.W. Nichols, C.W. Machan, Secondary-sphere effects in molecular electrocatalytic CO_2 reduction, Front. Chem. 7 (2019) 397, https://doi.org/10.3389/fchem.2019.00397.
[15] Y. Yao, J.-H. Wu, G. Liu, R. Zhang, Z.-S. Yang, S. Gao, T.-C. Lau, J.-L. Zhang, A bio-inspired bimetallic Fe–M catalyst for electro- and photochemical CO_2 reduction, ChemCatChem 16 (2024) e202301705, https://doi.org/10.1002/cctc.202301705.
[16] K. Rickmeyer, M. Huber, C.R. Hess, Influence of a neighbouring Cu centre on electro- and photocatalytic CO_2 reduction by Fe-Mabiq, Chem. Commun. 60 (2024) 819–822, https://doi.org/10.1039/d3cc04777f.
[17] M. Huber, A. Kumar, J. Hauer, E. Thyrhaug, C.R. Hess, Photoredox capacity expanded by the Cu site of CuFe-Mabiq, Chem. Commun. 61 (2025) 5731–5734, https://doi.org/10.1039/d4cc06104g.
[18] H.S. Stark, P.J. Altmann, S. Sproules, C.R. Hess, Structural characterization and photochemical properties of mono- and bimetallic Cu-Mabiq complexes, Inorg. Chem. 57 (2018) 6401–6409, https://doi.org/10.1021/acs.inorgchem.8b00471.
[19] P. Banerjee, A. Company, T. Weyhermüller, E. Bill, C.R. Hess, Zn and Fe complexes containing a redox active macrocyclic biquinazoline ligand, Inorg. Chem. 48 (2009) 2944–2955, https://doi.org/10.1021/ic8020172.
[20] O.C. Gagné, F.C. Hawthorne, Empirical Lewis acid strengths for 135 cations bonded to oxygen, Acta Crystallogr. Sect. B: Struct. Sci. Cryst. Eng. Mater. 73 (2017) 956–961, https://doi.org/10.1107/S2052520617010988.
[21] N.G. Léonard, T. Chantarojsiri, J.W. Ziller, J.Y. Yang, Cationic effects on the net hydrogen atom bond dissociation free energy of high-valent manganese imido complexes, J. Am. Chem. Soc. 144 (2022) 1503–1508, https://doi.org/10.1021/jacs.1c09583.
[22] S. Das, A. Roy, N. Chakrabarti, N. Mukhopadhyay, A. Sarkar, S. Sen Gupta, Self-sensitized Cu(II)-complex catalyzed solar driven CO_2 reduction, Chem. Sci. 16 (2025) 3114–3123, https://doi.org/10.1039/d4sc06354f.
[23] S.Y. Manafe, N. Le, E.C. Lambert, C. Curiac, D. Nugegoda, S. Das, L.A. Hunt, F. Qu, L.M. Whitt, I. Fedin, N.I. Hammer, C.E. Webster, J.H. Delcamp, E.T. Papish, Sensitized and self-sensitized photocatalytic CO_2 reduction to HCO_2^- and CO under visible light with Ni(II) CNC-pincer catalysts, ACS Catal. 14 (2024) 6589–6602, https://doi.org/10.1021/acscatal.3c03787.